Technical Note

Measurement and Characterization of RF Nonuniformity Over the Heart at 3T Using Body Coil Transmission

Kyunghyun Sung, MS* and Krishna S. Nayak, PhD

Purpose: To measure and characterize variations in the transmitted radio frequency (RF) (B1+) field in cardiac magnetic resonance imaging (MRI) at 3 Tesla. Knowledge of the B1+ field is necessary for the calibration of pulse sequences, image-based quantitation, and signal-to-noise ratio (SNR) and contrast-to-noise ratio (CNR) optimization.

Materials and Methods: A variation of the saturated double-angle method for cardiac B1+ mapping is described. A total of eight healthy volunteers and two cardiac patients were scanned using six parallel short-axis slices spanning the left ventricle (LV). B1+ profiles were analyzed to determine the amount of variation and dominant patterns of variation across the LV. A total of five to 10 measurements were obtained in each volunteer to determine an upper bound of measurement repeatability.

Results: The amount of flip angle variation was found to be 23% to 48% over the LV in mid-short-axis slices and 32% to 63% over the entire LV volume. The standard deviation (SD) of multiple flip angle measurements was $<1.4°$ over the LV in all subjects, indicating excellent repeatability of the proposed measurement method. The pattern of in-plane flip angle variation was found to be primarily unidirectional across the LV, with a residual variation of $\leq 3\%$ in all subjects.

Conclusion: The in-plane B1+ variation over the LV at 3T with body-coil transmission is on the order of 32% to 63% and is predominantly unidirectional in short-axis slices. Reproducible B1+ measurements over the whole heart can be obtained in a single breathhold of 16 heartbeats.

Key Words: cardiac MRI; RF nonuniformity; saturated double angle method; high-field MRI; prescan calibration
J. Magn. Reson. Imaging 2008;27:643–648.

Magnetic Resonance Engineering Laboratory, Ming Hsieh Department of Electrical Engineering–Systems, University of Southern California, Los Angeles, California, USA.

Contract grant sponsor: James H. Zumberge Foundation; Contract grant sponsor: American Heart Association; Contract grant number: 0435249N; Contract grant sponsor: National Institutes of Health; Contract grant numbers: R01-HL074332, R21-HL079987.

*Address reprint requests to: K.S., Research Assistant, 3740 McClintock Ave, EEB 412, University of Southern California, Los Angeles, CA 90089-2564.
E-mail: kyunghsu@sipi.usc.edu

Received January 3, 2007; Accepted October 2, 2007.
DOI 10.1002/jmri.21253
Published online 8 January 2008 in Wiley InterScience (www.interscience.wiley.com).

AS CARDIAC MRI moves to higher field strengths such as 3T, imaging protocols require careful consideration of possible nonuniformity of the transmitted radio frequency (RF) (B1+) field. Knowledge of this nonuniformity is crucial for pulse sequence calibration, image-based quantitation (such as in first-pass myocardial perfusion imaging), signal-to-noise ratio (SNR) and contrast-to-noise ratio (CNR) optimization, and the design of new pulse sequences. Estimated variations of 30% to 50% in the B1+ field over the heart at 3T have been reported in the literature (1–3). However, the analysis of in vivo B1+ variations in the chest has been limited by the lack of time-efficient B1+ mapping techniques.

There are several existing methods for B1+ mapping in static body regions (2–8). One of the simplest and the most straightforward methods is the double angle method (DAM) (6,7), which involves acquiring images with two nominal flip angles (operator prescribed values) α and 2α. The method uses the trigonometric double angle formula to determine the true flip angle and requires a long repetition time ($TR \gg T1$) to ensure full relaxation before α and 2α pulses.

Cunningham et al (3) recently proposed the saturated double-angle method (SDAM), which permits rapid B1 mapping with $TR < T1$. A saturation pulse at the end of each data acquisition resets the longitudinal magnetization to a known state. The B1+ field is still derived from the ratio of signal magnitudes after α and 2α pulses. SDAM with $TR < T1$ was successfully validated against DAM with $TR \gg 5T1$ in phantoms and static body regions. The feasibility of rapid cardiac B1 mapping was shown but the methodology was susceptible to irregular heart rates and B0 and B1 variation.

In this work, we implemented a variation of SDAM for B1+ measurement across the entire heart in a single breathhold by considering the B0 and B1 sensitivity of saturation pulses, possible variations in heart rate, and possible cross-talk between slices in a multislice acquisition. We measured and analyzed whole-heart B1+ profiles from 10 subjects using two 3T scanners with body-coil transmission. Repeatability testing was performed to determine practical utility of the measurement methodology for prescan calibration. Profile analysis was performed to determine patterns of variation that may be exploited during B1+ shimming.

MATERIALS AND METHODS

Cardiac SDAM

Successful multislice cardiac B1+ measurement at 3T using SDAM requires: 1) robust magnetization saturation in the presence of the B0 and B1+ inhomogeneity; 2) identical saturation recovery time (T_{SR}) even during irregular heartbeats (R-R intervals); and 3) minimization of cross-talk between adjacent slices in an interleaved multislice acquisition.

To address the first issue, we examined the effectiveness of various saturation pulses. The performance of saturation pulses as a function of B0 and B1+ inhomogeneity was investigated (3), and we selected an adiabatic composite pulse (BIR-4) (9) to support a B0 bandwidth of ± 130 Hz, typical for 3T cardiac imaging (10). Although the BIR-4 pulse (8 msec) has longer pulse duration and higher RF power than conventional pulses, its effects are minimal in this work because the pulse is applied only once per R-R interval and its duration is relatively small compared to the total image acquisition time (80 msec).

The second issue deals with variations in the R-R interval. When the saturation pulse is timed at the end of data acquisition (3), even a small change in heart rate produces variation in T_{SR}, causing an error in the true flip angle calculation. In this work, we timed the saturation pulse with a prospective triggering signal to make T_{SR} independent of heart rate, producing more robust B1+ maps.

The third issue deals with multislice acquisitions, for which B1+ measurements may be affected by flow-induced cross-talk between slices. If a TR for each slice is too long or an interslice gap is too small, cross-talk can occur because the through plane flow can reach to the next slice to be imaged. The maximum through plane flow (V_{max}) without cross-talk can be derived from the interslice gap (SG) and TR,

$$V_{\max} \leq \frac{SG}{TR}. \qquad (1)$$

We implemented a short multislice acquisition and enforced a minimum gap of 15 mm. For TR of 11 msec, this gap completely avoids cross-talk for through plane velocities in the left ventricle (LV) up to 1.36 m/second.

The pulse sequence, shown in Fig. 1, consists of three modules. The RESET module is timed with the gating signal, and consists of a BIR-4 saturation pulse (8 msec) followed by a gradient spoiler. The FATSAT module consists of a fat-selective excitation (8 msec) followed by a gradient spoiler. The IMAGING module consists of a slice-selective excitation, a 5.9-msec spiral readout, and a gradient spoiler. T_{SR} begins at the end of the RESET module. T_{SR} for slice #1 was set to 300–400 msec for plethysmograph gating and 500–600 msec for electrocardiograph (ECG) gating, depending on the heart rate.

The flip angle calculation in the double angle approach (3,6–8) follows:

$$\hat{\alpha}(x,y) = \arccos\left(\frac{I_{2\alpha}(x,y)}{2I_{\alpha}(x,y)}\right), \qquad (2)$$

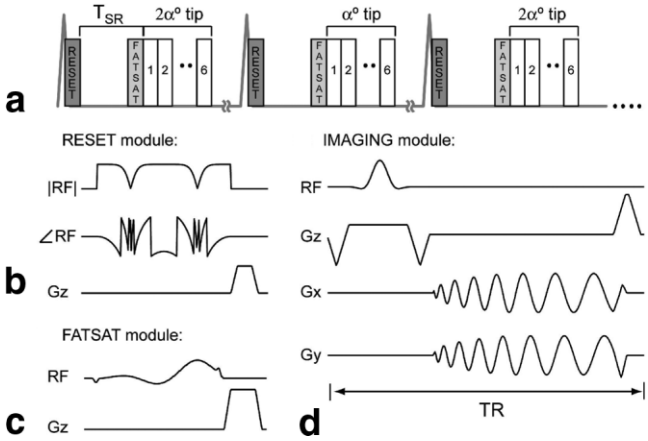

Figure 1. Cardiac SDAM pulse sequence. Full images are acquired with a nominal 2α and nominal α flip angle. **a:** Acquisitions are cardiac gated in a single breathhold to prevent motion artifacts, and consist of a magnetization reset, delay (T_{SR}), fat saturation, and multislice acquisition. **b:** The RESET module consists of an 8-msec BIR-4 saturation pulse followed by a dephaser. **c:** The FATSAT preparation consists of a fat-selective saturation followed by a dephaser. **d:** The IMAGING module consists of a slice-selective excitation, a short spiral readout (5.9 msec), and a dephaser. Note that the IMAGING excitation is slice selective, while the RESET and FATSAT excitations are not spatially-selective.

where $\hat{\alpha}(x,y)$ is the measured flip angle map and $I_{\alpha}(x,y)$ and $I_{2\alpha}(x,y)$ are the base magnitude images with the nominal flip angle of α and 2α. Image nonuniformities except for the flip angle–induced variation are identical for both base magnitude images, and therefore will be cancelled out in Eq. [2].

Since $I_{\alpha}(x,y)$ and $I_{2\alpha}(x,y)$ contain image noise, $\hat{\alpha}(x,y)$ can be decomposed into the true flip angle map $\alpha(x,y)$ and an additional noise term $n_{\alpha}(x,y)$

$$\hat{\alpha}(x,y) = \alpha(x,y) + n_{\alpha}(x,y), \qquad (3)$$

where $n_{\alpha}(x,y)$ can be analyzed using second order statistics: mean $E(n_{\alpha}(x,y))$ and standard deviation (SD) $\sigma_{n_{\alpha}}(x,y)$. Both $E(n_{\alpha})$ and $\sigma_{n_{\alpha}}$ depend on α and the base image SNR. $\sigma_{n_{\alpha}}$ and $E(n_{\alpha})$ were simulated as a function of α with different base image SNRs. According to simulations for a base image SNR range of 70–120, $\hat{\alpha}$ was close to α with relatively small $\sigma_{n_{\alpha}}$ and $E(n_{\alpha})$, when α was larger than 20°.

Experimental Methods

Experiments were performed on two identical GE Signa 3.0T EXCITE systems (General Electric Healthcare, Waukesha, WI, USA) with gradients capable of 40 mT/m amplitude and 150 T/m/second slew rate, and receivers supporting 4-μsec sampling (±125 kHz). Quadrature birdcage body coils (60-cm diameter and 32 rungs) were used for RF transmission and an eight-channel cardiac phased array coil was used for signal reception. Parallel imaging was not used. The transmit gain was calibrated using the vendor-supplied prescan process. The acquisition parameters were as follows:

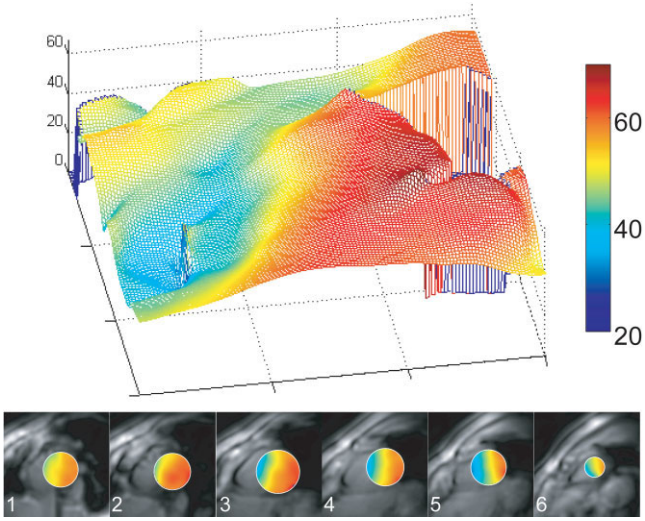

Figure 2. Cardiac flip angle maps from one representative volunteer at 3T. All six short-axis slices were acquired in a single 16 R-R breathhold. A mesh plot (top) depicting the flip angle variation in a mid-short-axis slice (slice #3) and flip angle profiles (bottom) in all six slices. Magnitude images with a nominal flip angle of 60° are provided for anatomical reference. Note that the variation appears strong and primarily unidirectional.

sinc RF pulse = 2.6 msec, TE = 2 msec, TR = 11 msec, field of view (FOV) = 30 cm, in-plane resolution = 2.2 mm, and slice thickness = 5 mm. Only the first 1.9 msec of each spiral readout was used during reconstruction by applying an appropriately-sized Hamming window to the raw k-space data. This increased the base image SNR while reducing the in-plane spatial resolution to 5 mm.

Cardiac B1+ measurements were acquired in eight healthy volunteers and two cardiac patients (eight males and two females, ages = 24–71 years, weights = 55–86 kg, resting heart rates = 49–81 bpm). The imaging protocols were approved by the Institutional Review Board of the University of South Carolina. Each subject was screened for MRI risk factors and provided informed consent in accordance with institutional policy. Scan plane localization was performed using the GE I-drive real-time system. In each volunteer, six parallel short-axis slices were prescribed spanning the LV from base to apex. The basal slice was denoted as #1 and the apical slice was denoted as #6. Whole-heart B1+ mapping was achieved in a single breathhold of 16 R-R intervals. Synchronization with the cardiac cycle was achieved with prospective triggering based on either an infrared plethysmograph (five subjects) (11) or an ECG (five subjects) signal.

A total of 10 repeated measurements were obtained in each of the healthy volunteers and five repeated measurements were obtained in each of the cardiac patients in separate breathholds with the same scan plane prescription. Subjects were instructed to perform each breathhold in a comfortable exhaled position. The subjects had no prior training for consistent breathhold positioning. Measurements containing at least one missed trigger were excluded from the data analysis, resulting in eight to 10 useful scans for each of the normal volunteers and five useful scans for each of the patients.

Data Analysis

All data analysis was performed in MATLAB 7.0 (The Mathworks, Natick, MA, USA). Circular regions of interest (ROIs) covering left ventricular myocardium and blood pool were manually defined based on magnitude images. Based on $\hat{\alpha}(x,y)$, the percentage of flip angle variation was defined as

$$Variation = \frac{\hat{\alpha}_{\max} - \hat{\alpha}_{\min}}{\hat{\alpha}_{\max}} \times 100\%. \quad (4)$$

We computed the mean and SD across measurements on the same subject and under the same conditions (imaging parameters and scan plane). The repeatability test determined an upper bound of measurement repeatability and indicated the usefulness of the technique for prescan calibration. Factors that likely contributed to the variation in measurements were $n_\alpha(x,y)$ and inconsistent breathhold positions. Pixel-by-pixel mean $E(\hat{\alpha}(x,y))$ and SD $\sigma_{\hat{\alpha}}(x,y)$ of the flip angle maps based on the five to 10 measurements were computed to provide the repeatability. The pixel based $\sigma_{\hat{\alpha}}(x,y)$ was then averaged over the ROI to produce a single number:

$$A = E(\sigma_{\hat{\alpha}}(x,y)),\ x,y \in ROI, \quad (5)$$

as an indicator of overall repeatability.

After observing that the in-plane flip angle variations were primarily unidirectional over the LV, we attempted to model the measured flip angle profile, $\hat{\alpha}(x,y)$, with a 1D approximation in each short-axis slice. We computed minimum mean squared error (MMSE) 1D approximations, $\hat{\alpha}(x')$, for in-plane orientation with a 1° increment and defined the primary in-plane axis as the one that minimized the approximation error, B:

$$B = E\left(\frac{|\hat{\alpha}(x,y) - \hat{\alpha}(x')|}{|\hat{\alpha}(x,y)|}\right) \times 100\%, \quad x,y \in ROI. \quad (6)$$

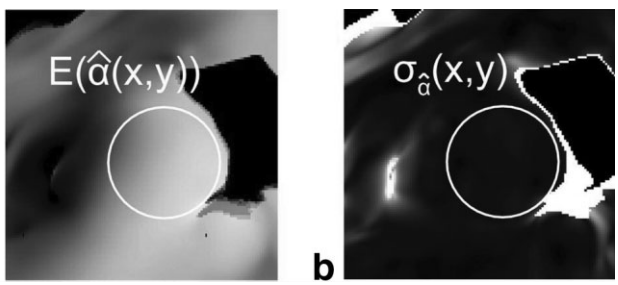

Figure 3. Illustration of repeatability analysis. Pixel-by-pixel (**a**) mean (gray scale 20°–70°) and (**b**) SD (0°–10°) of the measured flip angle map in a short-axis slice (slice #3 in subject #1). The metric A is computed by averaging $\sigma_{\hat{\alpha}}(x,y)$ over the ROI (white circle).

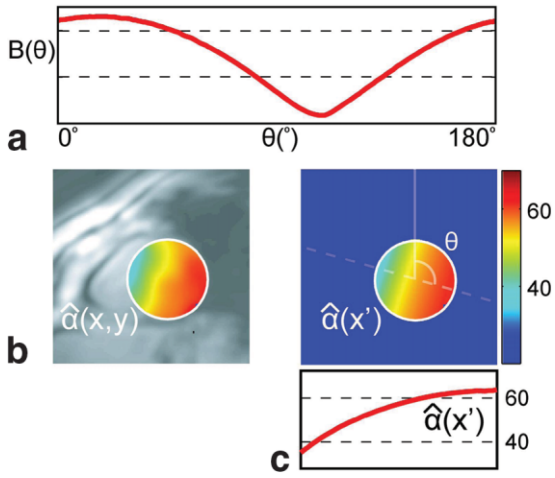

Figure 4. Illustration of profile analysis. **a:** The approximation error, $B(\theta)$, as a function of in-plane angle θ, defined in degrees clockwise from the vertical axis. **b:** Flip angle variation $\hat{\alpha}(x,y)$ in a circular ROI can be approximated by (**c**) a 1D function $\hat{\alpha}(x')$ along the primary in-plane axis (dotted line). The primary in-plane axis angle is 108° and the approximation error is 1.2% in this example (slice #3 in subject #1).

RESULTS

Representative flip angle maps for all six short-axis slices in one healthy volunteer are shown in Fig. 2. For a nominal flip angle of 60°, the observed flip angles across the LV myocardium ranged from 32° to 64°. The percentage variations within 2D short-axis slices ranged from 29% to 48% in this volunteer. One can qualitatively observe that the flip angle variation appears to be significant, smooth, and primarily along one in-plane axis.

Figure 3 illustrates the measurement repeatability testing. The pixel-by-pixel mean $E(\hat{\alpha}(x,y))$ is assumed to be close to true flip angle profile $\alpha(x,y)$, and $\sigma_{\hat{\alpha}}(x,y)$ depicts the variation among measurements. The pixel-by-pixel SD within the ROI was less than 1.0° in 90% of pixels (0° is black, 10° is white). High-pixel SD values exist at the epicardial border and the edge of the chest wall due to inconsistencies in breathhold position. The average SD metric, A, was less than 1.4° in all subjects, which suggests that the measurement methodology produces highly repeatable results.

Figure 4 illustrates the profile analysis used to determine the dominant direction of variation. The vertical line was selected from the magnitude image and the in-plane angle (θ) was defined as a clockwise angle from the vertical line to an axis of variation in degrees. The approximation error as a function of θ has one clear minima, which indicates a unique primary axis of variation. The approximation errors between the true (2D) profile and "best" unidirectional (1D) approximation were $\leq$3.1% in all subjects, and were $\leq$1.5% in eight of the subjects. The observed profiles were consistent for both 3T scanners.

Figure 5 contains mid-short-axis flip angle maps and illustrates the ROI analysis for all 10 subjects. Magnitude images (background) are shown for anatomical reference. The amount of flip angle variation over the 3D LV volume for the 10 subjects ranges from 31% to 66% while the flip angle variation over the LV in 2D mid-short-axis slices ranges from 23% to 53%. Flip angle maps from all subjects exhibit unidirectional variation along one primary in-plane axis.

Table 1 contains the statistical parameters for all subjects. Subjects 9 and 10 were cardiac patients. The average heart rate for the cardiac patients was 74 bpm and the average heart rate for the healthy subjects was 65 bpm. Subjects 7 and 8 were scanned in a different scanner than the other subjects.

DISCUSSION

The observed unidirectional trend at 3T may be used to compensate in-plane B1+ inhomogeneity using tailored radiofrequency (TRF) pulses (12,13). The presence of unidirectional in-plane B1+ variation greatly simplifies the design of compensating pulses, and enables the design of exceptionally short pulses (13). Further reductions in the duration of compensating pulses can be accomplished using parallel RF transmission (14).

The IMAGING module can incorporate spin-echo schemes or alternate k-space segmentations such as echo planar imaging (EPI). Spin-echo approaches are able to refocus T2* related inhomogeneities and may provide better noise behavior at lower flip angles (8) but are difficult to combine with interleaved multislice imaging. Although spiral readouts were chosen due to their efficiency and short echo time to reduce T2* effects, EPI readouts may also be used.

The cardiac B1+ measurement may have an important clinical role during prescan calibration at 3T. Kim

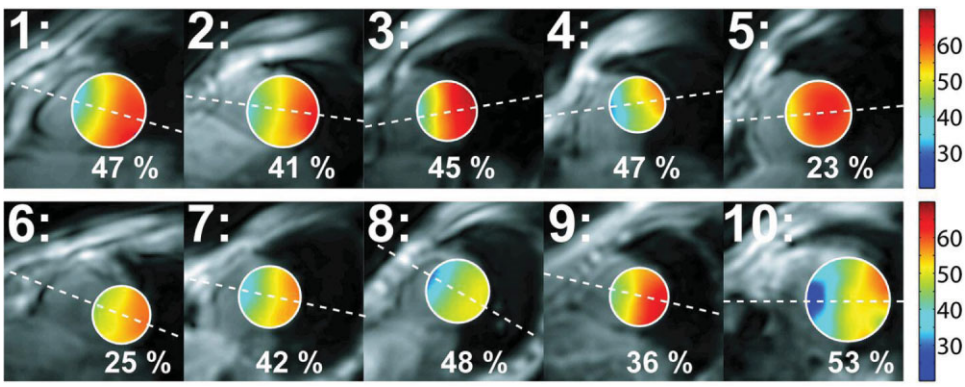

Figure 5. Mid-short-axis B1+ maps in all 10 subjects (eight healthy volunteers: 1–8 and two cardiac patients: 9 and 10). Magnitude images with a nominal flip angle of 60° are included for anatomical reference. Within each ROI (white circle), the primary in-plane axis of variation is indicated (dotted line). The flip angle variation in mid-short-axis slices was found to be 23% to 53%.

Table 1
Repeatability and Profile Analysis Data From all 10 Subjects

Subject #	Mid-short-axis 2D slice				3D volume[a]			
	A (°)[b]	*B* (%)[c]	$\alpha_{min} - \alpha_{max}$ (°)[d]	Variation(%)[e]	*A* (°)[b]	*B* (%)[c]	$\alpha_{min} - \alpha_{max}$ (°)[d]	Variation (%)[e]
1	0.6	1.2	34–64	47.1	0.8	1.1	32–64	50.2
2	0.6	1.2	36–62	41.3	0.6	1.5	34–64	46.0
3	0.6	0.8	37–67	44.9	0.9	1.1	34–67	49.4
4	1.4	1.9	31–58	47.0	1.4	2.1	26–59	55.6
5	0.4	1.0	48–63	23.0	0.5	1.1	45–66	31.3
6	1.0	1.2	44–59	25.2	1.0	1.2	42–61	31.2
7	0.8	1.4	30–57	48.0	0.8	1.4	28–58	52.2
8	0.9	1.5	38–65	41.6	1.1	1.4	34–67	49.0
9	0.5	1.5	42–66	36.0	0.6	1.2	42–66	36.0
10	1.4	3.1	27–58	52.5	1.3	3.0	20–60	65.7

[a]3D volume parameters include all six slices in the analysis.
[b]*A* represents the average SD of the measured flip angle (in degrees) over the LV ROI, and is an indicator of overall repeatability.
[c]*B* represents the relative approximation error between the true (2D) pattern and the unidirectional (1D) approximation along the primary in-plane axis of variation.
[d]α_{max} and α_{min} are the maximum and minimum measured flip angle over the LV ROI.
[e]Variation is calculated as $(\alpha_{max} - \alpha_{min})/\alpha_{max}$ in percentage.

et al (15) demonstrated that B1+ inhomogeneity can result in regional contrast variations across the heart. Uniform saturation may potentially be achieved if cardiac B1+ measurements are used to guide the choice of B1 amplitude. Knowledge of the B1+ field may also improve the calibration of time–intensity curves in first-pass myocardial perfusion imaging along with several existing methods to correct intensity variations (16,17). Finally, an ideal flip angle in balanced steady-state free precession (SSFP) imaging is often precalculated to achieve the highest contrast between tissues (18) and this contrast can be further optimized with B1+ mapping.

Off-resonance effects during excitation and readout can be considered separately. Off-resonance during slice-selective excitation creates a small distortion in the excited slice profile but the distortion is independent of the RF amplitude. Off-resonance effects during spiral acquisitions can cause image blurring when the amount of phase accrual during a readout is greater than $\pi/2$ (19). The truncated 1.9-msec spiral readout has a bandwidth of ± 132 Hz within which the phase accrual is less than $\pi/2$. Redesign of the BIR-4 saturation and data acquisition scheme may be needed for cardiac B1+ mapping in the presence of extreme off-resonance, caused by inadequate shimming, sternal wires or metal clips from prior surgery, or imaging at greater than 3T.

The measurement variations found here can be considered upper bounds on the true variation of the measurement methodology. Further improvements in repeatability may be achieved by 3D image registration and wavelet-based denoising (20), which could suppress contributions from breathhold inconsistency and the additive noise term. The difference in overall quality may be subtle due to the low image resolution in this work.

During acquisition, we used a spatial resolution of 2.2 mm with eight-interleaved 5.9-msec spiral readouts, and during data analysis we windowed k-space data, which reduced the effective resolution to 5 mm. In future studies, the same spatial resolution can be achieved with shorter 1.9-msec readouts and eight interleaves, or with 5.9-msec readouts and just three interleaves. The low resolution condition may assist to either shorten the breathhold duration (by a factor of 3) or increase the number of slices with the cross-talk–free through-plane velocities up to 2.14 m/second.

The trigonometric double angle formula (Eq. [2]) has a limited measurable bound. The arccosine function contains only a positive signal ratio, and therefore the derived value ranges from 0° to 90°. The calculation assumes a linear relationship between flip angles and B1+ fields and the deviation from the relationship must be taken into account for larger flip angles ($> 70°$) (7). In addition, the repeatability may become worse for smaller flip angles ($< 20°$ in this work). These limitations should be carefully considered when severe transmitted B1+ variation is expected.

In conclusion, this study has done the following: 1) verified that the proposed SDAM pulse sequence produces reproducible cardiac B1+ maps over the entire heart in a single breathhold; 2) shown the flip angle variation at 3T to be approximately 32% to 63% over the 3D left ventricle, and approximately 23% to 48% within 2D short-axis slices; and 3) established that the in-plane variation is primarily along one axis in short-axis slices.

REFERENCES

1. Singerman RW, Denison TJ, Wen H, Balaban RS. Simulation of B1 field distribution and intrinsic signal-to-noise in cardiac MRI as a function of static magnetic field. J Magn Reson 1997;125:72–83.
2. Greenman RL, Shirosky JE, Mulkern RV, Rofsky NM. Double inversion black-blood fast spin-echo imaging of the human heart: a comparison between 1.5T and 3.0T. J Magn Reson Imaging 2003; 17:648–655.
3. Cunningham CH, Pauly JM, Nayak KS. SDAM: saturated double angle method for rapid B1+ mapping. Magn Reson Med 2006;55: 1326–1333.
4. Hornak JP, Szumowski J. Magnetic field mapping. Magn Reson Med 1988;6:158–163.
5. Akoka S, Franconi F, Seguin F, Le Pape A. Radiofrequency map of an NMR coil by imaging. Magn Reson Imaging 1993;11:437–441.

6. Insko EK, Bolinger L. Mapping of the radiofrequency field. J Magn Reson 1993;103:82–85.
7. Stollberger R, Wach P. Imaging of the active B1 field in vivo. Magn Reson Med 1996;35:246–251.
8. Wang J, Qiu M, Yang QX, Smith MB, Constable RT. Measurement and correction of transmitter and receiver induced nonuniformities in vivo. Magn Reson Med 2005;53:408–417.
9. Staewen RS, Johnson AJ, Ross BD, Parrish T, Merkle H, Garwood M. 3-D FLASH imaging using a single surface coil and a new adiabatic pulse, BIR-4. Invest Radiol 1990;25:559–567.
10. Noeske R, Seifert F, Rhein KH, Rinneberg H. Human cardiac imaging at 3T using phased array coils. Magn Reson Med 2000;44:978–982.
11. Hokanson DE, Sumner DS, Strandness DE, Jr. An electrically calibrated plethysmograph for direct measurement of limb blood flow. IEEE Trans Biomed Eng 1975;22:25–29.
12. Saekho S, Boada FE, Noll DC, Stenger VA. Small tip angle three-dimensional tailored radiofrequency slab-select pulse for reduced B1 inhomogeneity at 3T. Magn Reson Med 2005;53:479–484.
13. Sung K, Cunningham CH, Nayak KS. Validation of B1+ nonuniformity correction in the chest at 3T using TIP-COMP. In: Proceedings of the 14th Annual meeting of ISMRM, Seattle, WA, USA, 2006 (Abstract 597).
14. Katscher U, Bornert P. Parallel RF transmission in MRI. Magn Reson Med 2003;49:144–150.
15. Kim D, Cernicanu A, Axel L. B0 and B1-insensitive uniform T1-weighting for quantitative, first-pass myocardial perfusion magnetic resonance imaging. Magn Reson Med 2005;54:1423–1429.
16. Hsu LY, Rhoads KL, Holly JE, Kellman P, Aletras AH, Arai AE. Quantitative myocardial perfusion analysis with a dual-bolus contrast-enhanced first-pass MRI technique in humans. J Magn Reson Imaging 2006;23:315–322.
17. Ruan C, Yang S, Cusi K, Gao F, Clarke GD. Correction of myocardial perfusion reserve data from first-pass MR imaging at 3.0 Tesla with parallel imaging. In: Proceedings of the 14th Annual meeting of ISMRM, Seattle, WA, USA, 2006 (Abstract 1167).
18. Schar M, Kozerke S, Fischer SE, Boesiger P. Cardiac SSFP imaging at 3 Tesla. Magn Reson Med 2004;51:799–806.
19. Noll DC, Pauly JM, Meyer CH, Nishimura DG, Macovski A. Deblurring for non-2d Fourier transform magnetic resonance imaging. Magn Reson Med 1992;25:319–333.
20. Donoho DL, Johnstone IM. Adapting to unknown smoothness via wavelet shrinkage. J Amer Stat Assn 1995;90:1200–1224.